



Embryonic development of the cricket *Gryllus bimaculatus*



Seth Donouge^a, Cassandra G. Extavour^{a,b,*}

^a Department of Organismic & Evolutionary Biology, Harvard University, 16 Divinity Avenue, Cambridge, MA 02138, United States

^b Department of Molecular & Cellular Biology, Harvard University, 16 Divinity Avenue, Cambridge, MA 02138, United States

ARTICLE INFO

Article history:

Received 13 November 2014

Received in revised form

10 April 2015

Accepted 11 April 2015

Available online 20 April 2015

Keywords:

Orthoptera

Hemimetabola

Staging

Embryogenesis

Morphogenesis

Germ band

Katatrepsis

Gryllus bimaculatus

Two-spotted cricket

Ensifera

ABSTRACT

Extensive research into *Drosophila melanogaster* embryogenesis has improved our understanding of insect developmental mechanisms. However, *Drosophila* development is thought to be highly divergent from that of the ancestral insect and arthropod in many respects. We therefore need alternative models for arthropod development that are likely to be more representative of basally-branching clades. The cricket *Gryllus bimaculatus* is such a model, and currently has the most sophisticated functional genetic toolkit of any hemimetabolous insect. The existing cricket embryonic staging system is fragmentary, and it is based on morphological landmarks that are not easily visible on a live, undissected egg. To address this problem, here we present a complementary set of “egg stages” that serve as a guide for identifying the developmental progress of a cricket embryo from fertilization to hatching, based solely on the external appearance of the egg. These stages were characterized using a combination of brightfield timelapse microscopy, timed brightfield micrographs, confocal microscopy, and measurements of egg dimensions. These egg stages are particularly useful in experiments that involve egg injection (including RNA interference, targeted genome modification, and transgenesis), as injection can alter the speed of development, even in control treatments. We also use 3D reconstructions of fixed embryo preparations to provide a comprehensive description of the morphogenesis and anatomy of the cricket embryo during embryonic rudiment assembly, germ band formation, elongation, segmentation, and appendage formation. Finally, we aggregate and schematize a variety of published developmental gene expression patterns. This work will facilitate further studies on *G. bimaculatus* development, and serve as a useful point of reference for other studies of wild type and experimentally manipulated insect development in fields from evo–devo to disease vector and pest management.

© 2015 Elsevier Inc. All rights reserved.

Introduction

The two-spotted field cricket, *Gryllus bimaculatus*, has long been used as a model for behavior, neurobiology, and physiology. More recently, it has emerged as a model for insect developmental genetics as well. *G. bimaculatus* is a member of the order Orthoptera, a group that branches basally with respect to the most extensively studied insect species, including the fruit fly *Drosophila melanogaster*, the flour beetle *Tribolium castaneum*, and the

silkworm *Bombyx mori*. It thus serves as a useful comparator for inferring events in the early evolutionary history of Insecta, and potentially even in the shared ancestor of Arthropoda or Bilateria.

G. bimaculatus development (summarized in Fig. 1) is unlike that of *D. melanogaster* in several respects. First, in *D. melanogaster*, as in many long germ insects, nearly all cells of the blastoderm form the embryo proper. In this case, the embryo fills the entire space within the vitelline membrane and surrounds the yolk throughout embryogenesis, leaving a small proportion of blastoderm cells that are fated to become *D. melanogaster*'s single extraembryonic membrane, called the amnioserosa. In contrast, typical of intermediate and short germ insects, only some of the cells of the *G. bimaculatus* blastoderm contribute to an embryonic rudiment that forms on the surface of the yolk. The remaining cells form two large and distinct extraembryonic membranes: the amnion, which lies on the ventral side of the embryo, and the serosa, which surrounds the embryo and yolk mass on the dorsal side (reviewed by Panfilio (2008)). Second, while *D. melanogaster* is a long germ insect that forms all of its body segments essentially simultaneously, *G. bimaculatus* is an intermediate germ insect, in

Abbreviations: A, anterior; A1, first abdominal segment; am, amnion; an, antenna/ae; cc, cercus/cerci; cho, chorion; co, coxopodite; D, dorsal; ect, ectoderm; ee, extra-embryonic region; end, endoderm; fe, femur; L, thoracic leg; la, labrum; LB, limb bud; me, mesectoderm; mes, mesoderm; mn, mandible; mx1, first maxilla; mx2, second maxilla; NB, neuroblast; ne, neuroectoderm; P, posterior; pp, pleuropodia; pr, proctodaeum; ser, serosa; st, stomodaeum; T1, first thoracic segment; ta, tarsus; te, telopodite; ti, tibia; V, ventral; VF, ventral furrow

* Corresponding author at: Department of Organismic & Evolutionary Biology, Harvard University, 16 Divinity Avenue, Cambridge, MA 02138, United States. Fax: +1 617 496 9507.

E-mail address: extavour@oeb.harvard.edu (C.G. Extavour).

<http://dx.doi.org/10.1016/j.ydbio.2015.04.009>

0012-1606/© 2015 Elsevier Inc. All rights reserved.

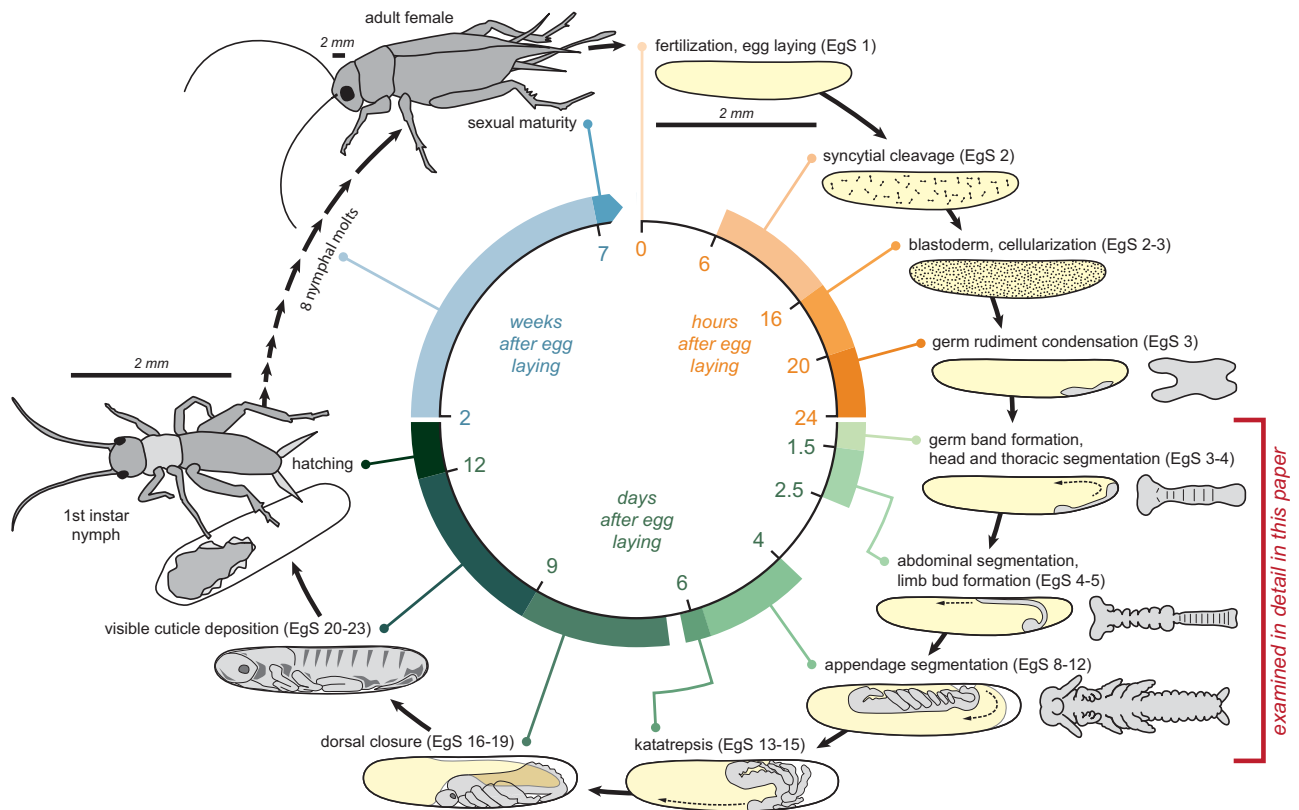


Fig. 1. Schematic of the *Gryllus bimaculatus* life cycle. Schematic drawings of selected embryonic and nymphal stages are shown, with the duration of each stage shown in hours (orange), days (green), or weeks (blue) after egg laying. Colored arcs indicate the window of time occupied by the indicated stage. Schematic drawings of embryogenesis show the position of the embryo (gray) within the egg relative to the yolk (yellow). Dotted lines with arrowheads indicate upcoming blastokinesis movements of the embryo. For stages examined in detail in this paper (bracketed in red), schematics on the left show morphologies of the embryo (gray) when dissected free from the yolk (yellow). "EgS" refers to egg stages defined in this paper. Live images of embryos at the stages corresponding to these schematics can be seen in time-lapse Movie S1 (EgS 1: 0 d 00:00 h–0 d 09:55 h; EgS 2: 0 d 10:00 h–0 d 15:15 h; EgS 3: 0 d 15:20 h–1 d 23:00 h; EgS 4: 1 d 23:05 h–2 d 12:10 h; EgS 5: 2 d 12:15 h–3 d 05:35 h) and Movie S2 (EgS 8–12: 4 d 01:45 h–6 d 11:50 h; EgS 13–15: 6 d 02:35 h–7 d 13:10 h; EgS 16–17: 7 d 11:15 h – end of Movie S2).

which head and thoracic segments are formed simultaneously and then abdominal segments are added sequentially as the anterior–posterior axis elongates. Third, unlike *D. melanogaster*, the cricket embryo changes its axial orientation while submerged within the yolk mass. This occurs in concert with morphogenetic movements of the two extraembryonic membranes in a two-part process termed blastokinesis (reviewed by Panfilio (2008)). The developing embryo completely reverses its anteroposterior orientation with respect to the eggshell once during anatrepsis (the first part of blastokinesis) and again during katatrepsis (the second part of blastokinesis) (Fig. 1). Fourth, crickets are hemimetabolous, which means that unlike the indirectly developing holometabolous insects, they do not pass through a larval stage nor go through total metamorphosis. Lastly, the *G. bimaculatus* ovary is panoistic. There are no germ line-derived nurse cells that provide cytoplasm to incipient oocytes; rather, each differentiating germ cell in females is thought to become an oocyte (Bünning, 1994). Based on the phylogenetic distribution of these features, many of these characteristics are likely ancestral to insects (Sander, 1997).

G. bimaculatus is easily cultured in the lab, and there are well-established protocols for observing gene expression and protein localization in whole mount embryos and organ systems of juveniles and adults. Two recently published transcriptomes (Bando et al., 2013; Zeng et al., 2013) have made it straightforward to identify genes of interests and use RNA interference (RNAi) to knock down maternal or zygotic transcripts (techniques reviewed by Mito and Noji (2009)). It is also possible to generate stable transgenic lines (Nakamura et al., 2010). Thanks to these tools, our understanding of a diverse array of long-standing problems in

arthropod and bilaterian evolution and development has improved, including limb development and regeneration (reviewed by Nakamura et al. (2008a)), segmentation (Kainz et al., 2011; Mito et al., 2011), anterior–posterior axis formation (Nakamura et al., 2010), novel gene evolution (Ewen-Campen et al., 2012), and germ cell specification (Donoughe et al., 2014). It is now also possible to perform site-directed genome editing (Watanabe et al., 2014, 2012), which opens up even more promising experimental possibilities.

All developmental studies, including those mentioned above, rely on a consistent embryonic staging system. A commonly used set of embryonic stages for *G. bimaculatus* was most recently updated by Mito and Noji (2009) and Kainz (2009), wherein embryonic stages are defined by morphological characteristics of the embryo. One drawback to the existing embryological staging system is that not all enumerated stages are defined by specific morphological features, and those that are well defined are limited to identification by examination of only a few organ systems. A second limitation of using these embryonic stages is that an embryo must be manually removed from the egg and examined in detail in order to identify its stage. This is because a large portion of cricket embryogenesis occurs when the embryo is submerged in yolk and the relevant morphological landmarks are not externally visible without this microdissection. Finally, although staging landmarks have been described for a number of other orthopterans (Bentley et al., 1979; Chapman and Whitham, 1968; Hägele et al., 2004; Harrat and Petit, 2009; Patel et al., 1989; Rakshpal, 1962; Riebert, 1961; Roonwal, 1936, 1937; Salzen, 1960; Sauer, 1961; Slifer and King, 1934; Slifer, 1932; Wheeler, 1893), it is not

clear how the *G. bimaculatus* stages correspond to those established for other crickets, grasshoppers, and locusts.

Our goal with this paper is therefore to facilitate embryological studies on *G. bimaculatus* by adding detail to the existing embryonic staging system, extending it to include stages that were not previously described, and presenting a complementary set of “egg stages” that makes it possible to determine the stage of a developing cricket embryo without removing it from its eggshell. This is particularly useful for eggs that have been injected, such as in zygotic RNAi experiments. A batch of injected embryos, even control-injected embryos, is often developmentally delayed compared to non-injected embryos (see e.g. Kainz et al. (2011)). Furthermore, injected eggs that are within two hours of the same chronological age can display a range of developmental stages that would normally correspond to those of embryos that were a few days apart in chronological age. This can lead to artifacts when interpreting the phenotypes obtained by RNAi, as developmental delays can be difficult to distinguish from developmental defects (see e.g. Kainz et al. (2011)). The egg stages described in this paper address this problem, as they make it possible to determine easily the developmental progress of an embryo based on external appearance alone and, if necessary, allow it to continue developing until it reaches the desired developmental stage of embryogenesis.

To show how egg stages can be used to determine the extent of development in cricket embryos, we include two time-lapse videos of wild type embryos, with accompanying descriptions of developmental events and the corresponding egg stages and embryonic stages. We also describe morphogenesis of the wild-type cricket embryo from the germ band stage through to late appendage segmentation stages, using 3D reconstructions and 2D projections of confocal micrographs to display external embryo morphology and optical sections to reveal internal embryo morphology. Finally, we summarize and schematize the expression patterns of a variety of cricket genes that are important for early embryogenesis, providing molecular landmarks that can be used to identify specific embryonic regions, organ primordia or tissue types during development.

Materials and methods

Animal husbandry and embryo collection

G. bimaculatus culture was founded in 2006 with animals purchased from LiveFoods Direct (Sheffield, United Kingdom). Since then, the colony has been kept as an inbred culture, maintained at 29 °C as previously described (Kainz et al., 2011). For precisely timed egg collections (embryo age range of five hours or fewer), adult females were provided with 6 cm petri dishes filled with fine sand (generic children’s sandbox sand, sieved to remove grains larger than ~200 µm) that was dampened with tap water and then covered with a thin layer of cotton (VWR #14224-514). Females insert their ovipositors through the cotton layer and lay eggs in the damp sand. After the collection period, the cotton was discarded, removing any accumulated frass or detritus in the process. Eggs were collected by washing the egg-laden sand through a 200-µm nylon sieve with tap water. Sand grains passed through the sieve while the eggs remained. The eggs were then washed into a glass beaker and rinsed several times with additional tap water to remove debris and any remaining sand. For roughly timed egg collections (age ranges greater than five hours), females were provided with 6-cm petri dishes filled with moistened cotton. After the collection period, eggs were washed free of cotton into a glass beaker using tap water, rinsed, and collected into a fresh petri dish as described for sand-collected eggs. Eggs collected using either method were aged in a 29 °C incubator until

they reached the desired stage. Eggs were aged while submerged in tap water, either en masse in a petri dish or individually in 6- or 12-well plates (Thermo Scientific #150628 and #140675; these need not be sterile and can be washed and reused). After ~12 d in water, eggs were moved to a fresh petri dish with Whatman filter paper laid over moistened cotton, which allowed crickets to hatch into air.

Egg measurements

To establish an egg staging scheme, sexually mature mated females were allowed to lay eggs in cotton-filled petri dishes for several hours. During this period the females cleared any previously fertilized older eggs that they may have been retaining in their uteri. This was followed by a one-hour egg collection into damp sand as described above. Eggs were individually incubated at 29 °C in 12-well plates filled with tap water. Half of the tap water was changed out every two or three days. Every six hours for 12 consecutive days, each egg was taken to a 25 °C room, where it was photographed from lateral, ventral, and dorsal views. Following these 12 d, eggs were moved to moist Whatman paper and checked for hatching every 12 h for two more days. A custom ImageJ macro was used to crop and orient all images for ease of analysis, and another custom macro was used to automatically extract approximate egg dimension data (Supplementary Fig. S2). ImageJ macros are available upon request.

In situ hybridization and immunostaining

Embryos were dissected, fixed, and subjected to in situ hybridization as previously described (Kainz et al., 2011). Embryos were counterstained with 1:500 or 1:1000 Hoechst 33342 (Sigma #B2261) 1–10 µg/mL.

Microscopy and image analysis

We recorded time-lapses covering the first two-thirds of embryogenesis, and annotated them with descriptions of developmental events, egg age, egg stage, and approximate embryonic stage (Movies S1 and S2). For time-lapse imaging of embryos up to egg stage 7 (beginning of egg expansion), eggs were secured to the bottom of a 3-cm petri dish using heptane glue (made by incubating Scotch 3M double-sided sticky tape in heptane) and covered with halocarbon oil 700 (Sigma #H8898) for imaging. We found that egg expansion (egg stages 7–9) failed to occur under halocarbon oil, although embryonic development proceeded normally in other respects for several hours. Therefore, for time-lapse imaging at egg stage 7 and beyond, embryos were placed in a trough cut into a block of Sylgard 184 elastomer (Dow Corning Sylgard 184 Elastomer Kit) and covered with tap water. Images were captured every five minutes for a period of up to five consecutive days under these conditions using AxioVision version 4.8 (Zeiss) driving a Zeiss Stereo Lumar microscope with an AxioCam MRc camera. Images were assembled into movies and annotated using ImageJ and Adobe After Effects CS5.

Supplementary material related to this article can be found online at [doi:10.1016/j.ydbio.2015.04.009](https://doi.org/10.1016/j.ydbio.2015.04.009).

The same microscope and control software used for time-lapse imaging were also used to take single time point micrographs. Since the sampling was performed at discrete points rather than continuously, the exact interval for each egg stage could not be measured and had to be estimated. Thus, there is ± 3 h (one half of the sampling interval) uncertainty for the beginning and end of each egg stage. Supplementary Fig. S1 contains information for each egg stage, including bright field egg images, description, schematic, duration, and correspondence to embryonic stages. This figure also contains an

updated list of embryonic stages and a brief summary of the characteristic developmental events of each stage.

For fixed embryo preparations, images were captured with AxioVision version 4.8 (Zeiss) driving a Zeiss AxioImager microscope with an AxioCam MRm camera and Apotome. Confocal microscopy of fixed preparations was performed with a Zeiss LSM 710 or LSM 780 microscope. External embryonic morphology, as shown in Figs. 5–9, was illustrated by staining fixed embryo

preparations with the nuclear dye Hoechst 33342 and taking optical confocal sections. The LSM Image VisArt plus module in Zen 2009 or 2011 (Zeiss) was used to render optical sections as a 3D structure illuminated by a virtual light source from above (mode: “shadow projection”) or from the rear (mode: “transparent projection”). Other image analyses and assembly were performed with AxioVision version 4.8, Helicon Focus Pro version 4.1.1 (HeliconSoft), Adobe Photoshop, Illustrator, and InDesign CS5.

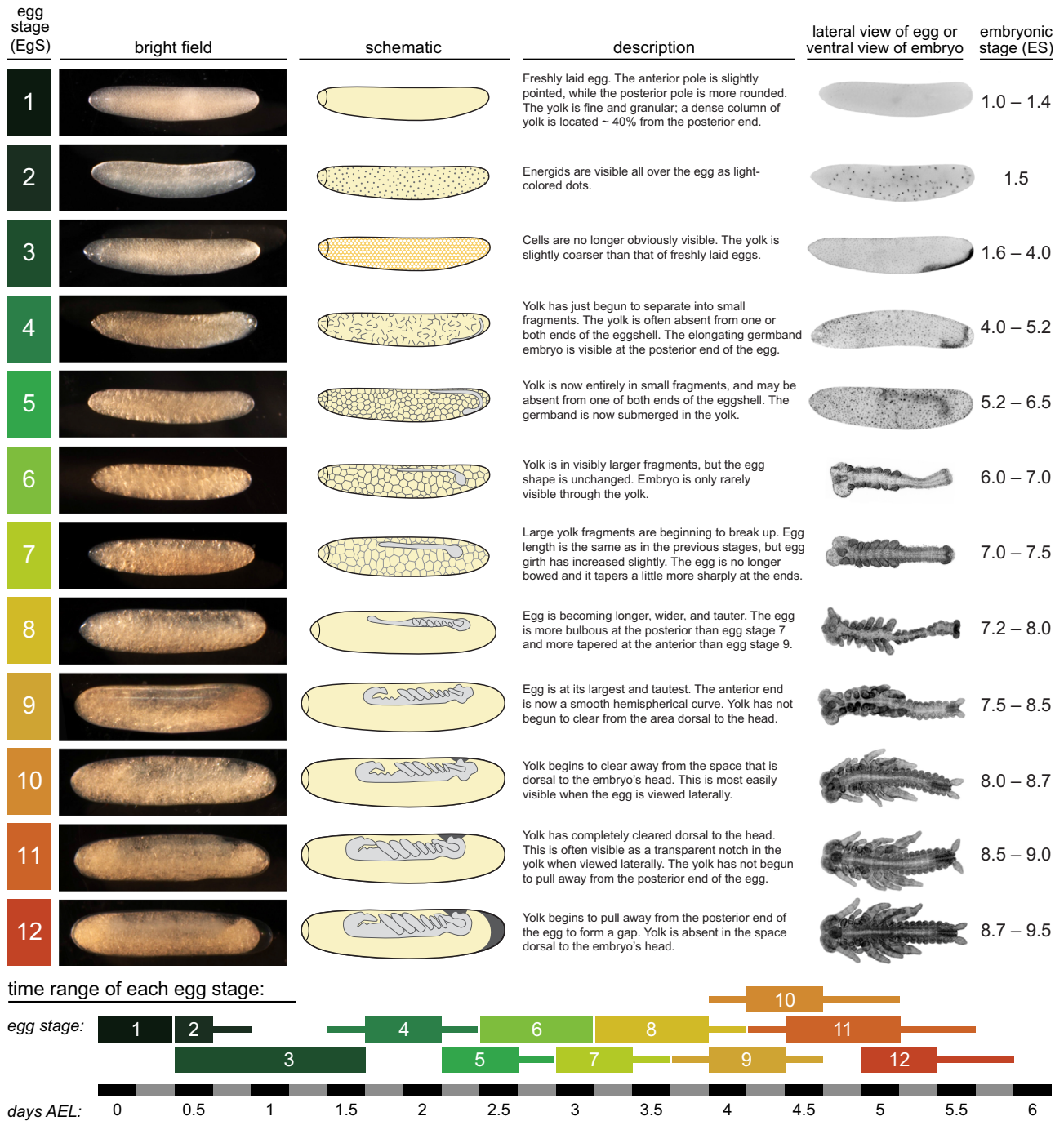


Fig. 2. Egg staging system for *G. bimaculatus* (EgS 1–12). Lateral views of representative individuals are shown to illustrate the egg morphology features that can be used to assign embryos to an egg stage (left), and the corresponding embryonic morphology and embryonic stages found within eggs of a given egg stage (right). Embryonic stages are as previously defined in the literature (Miyawaki et al., 2002, 2004; Niwa et al., 2000, 1997; Sarashina et al., 2005; Sato and Tanaka-Sato, 2002; Zhang et al., 2005), most recently summarized by Mito and Noji (2009) and Kainz (2009). Micrographs of live embryos at each stage are shown to the left of schematics showing morphologies and relative positions of the yolk (yellow) and the embryo (gray) at each stage. To the right of each text description is either a lateral view of a live H2B-GFP transgenic egg (EgS 1–5, 19–23) or a ventral view of a dissected and fixed embryo stained with the nuclear dye Hoechst 33342 (EgS 6–18). Micrographs have been inverted so that dark areas in the images represent strongest fluorescence intensity. The micrographs are not to scale. Timeline along bottom shows the range of time occupied by each egg stage, measured in days after egg laying (AEL) at 29 °C. At each time point, if at least one-third of eggs are at a given egg stage, the horizontal bar representing that egg stage is thick; if less than one-third of eggs are at that egg stage, the bar is thin.

Results and discussion

To complement and facilitate use of the descriptions of *G. bimaculatus* embryonic stages (ES) that have been described briefly in the literature (Kainz, 2009; Mito and Noji, 2009), we defined new egg stages (EgS) using characteristics that are externally visible when a wild type egg is illuminated with incident white light and examined with a dissection stereomicroscope. We collected 42 wild-type eggs that had been laid within a one-hour window and took a white light image of each one every six hours until hatching. We used these images to define distinct egg stages

(example images and schematics shown in Figs. 2 and 3; detailed descriptions follow below).

Once the egg stages were established, we examined the micrographs of all eggs at a given chronological age and assigned each individual to an egg stage. These data were used to make a timeline of embryonic development from egg laying through to hatching (Figs. 2 and 3, bottom). We found that cricket embryos can progress through development at slightly variable rates, even when they have been laid within only one hour of each other, and are raised under identical laboratory conditions. Development of embryos of the same age ± 30 min is largely synchronous through EgS 5, and then embryos begin to diverge. For example, embryos that simultaneously

egg stage (ES)	bright field	schematic	description	lateral view of egg or ventral view of embryo	embryonic stage (ES)
13			The cleared notch in the yolk is fully connected with the posterior gap, as the head emerges posteriorly from the yolk. None of the gnathal appendages are free from the yolk yet.		9.0 – 9.9
14			The midway point of katatrepsis. The legs are exposed in the yolkless space in the posterior of the egg.		10
15			Katatrepsis is complete, with the head now pointing anteriorly. A portion of the yolk forms a broad patch on the dorsal side of the embryo. When viewed ventrally, 55-60% of the egg is taken up by the embryo.		11
16			The patch of yolk narrows as dorsal closure begins. When viewed ventrally, 65-70% of the egg is taken up by the embryo. Eyes are lightly pigmented.		11
17			A bulge of yolk remains anterior to the embryo. When viewed ventrally, 80-85% of the egg is taken up by the embryo. Dorsal closure is well advanced in the abdomen. Eyes are more darkly pigmented.		11 – 12
18			The yolk has receded to a point slightly posterior to the anterior tip of the head.		11 – 12
19			The yolk is entirely posterior to the head, but a gap remains in the egg, anterior to the embryo. This gap is about the same size as in the previous stage.		12 – 13
20			Embryo begins to move forward, so that the gap anterior to the embryo is about half as large as in the previous stage.		12 – 14
21			Only a very small gap remains anterior to the embryo. Eyes are larger and darker. Pigment is now visible in the cuticle in other parts of the body, particularly the cerci.		13 – 14
22			No gap remains anterior to the embryo.		14
23			Embryo appears to have inflated, filling the volume of the egg shell completely. Cuticle is darker all over. Bristles are visible on legs, antennae, and on the dorsal side of the body.		15
24			Embryo hatches.		16

time range of each egg stage:

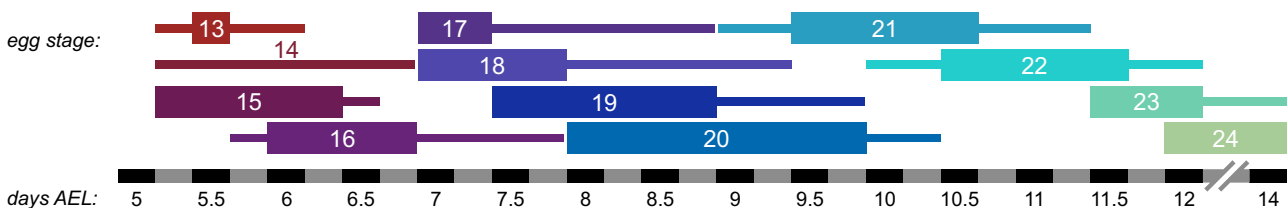


Fig. 3. Egg staging system for *G. bimaculatus* (EgS 13–24). Continued from Fig. 2.

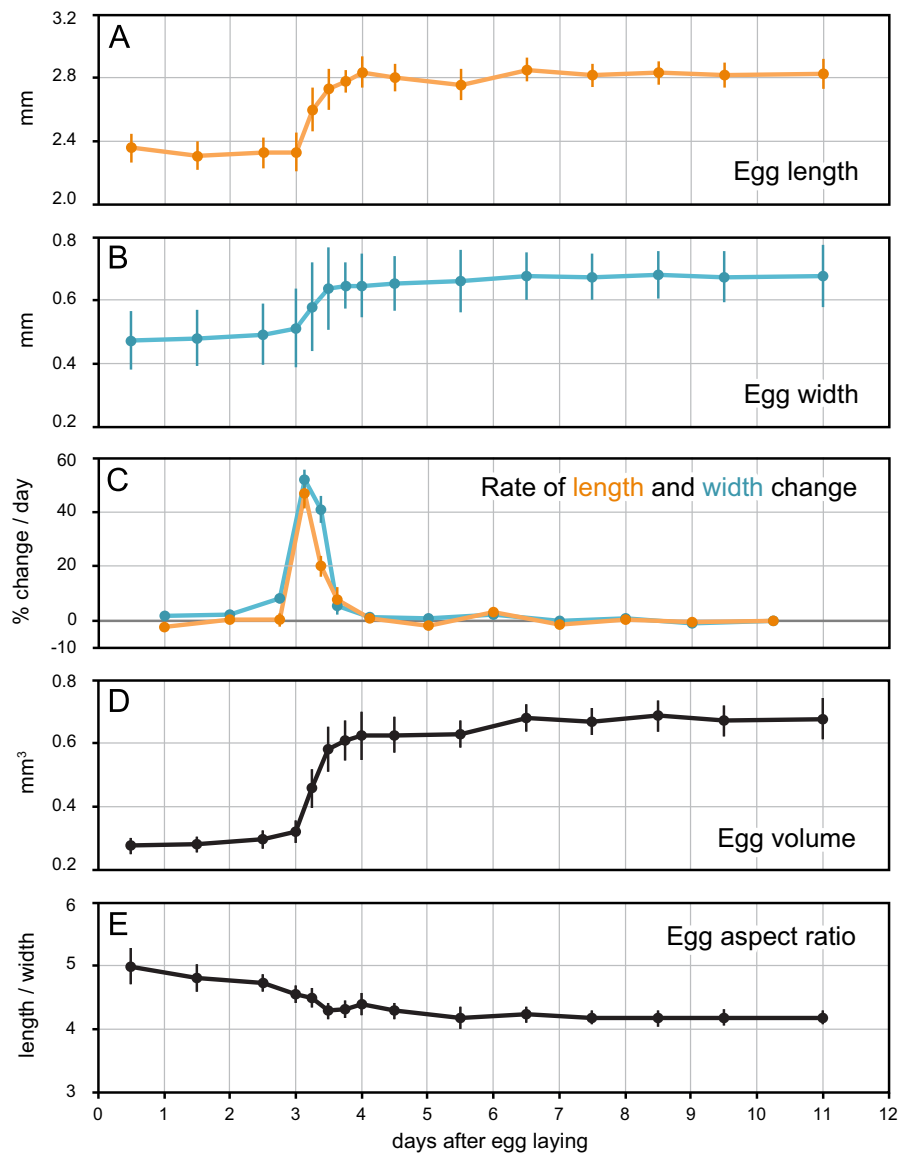


Fig. 4. Changes in egg sizes over time during early embryogenesis of *G. bimaculatus*. Length (A) and width (B) of ten eggs was measured manually from micrographs at a range of time points. From these measurements, we calculated the rate of change of length and width (C), the egg volume (D), and the aspect ratio as a function of days after egg laying (E).

reach EgS 5 might reach EgS 20 as much as 36 h apart from one another. Embryonic mortality is more frequent towards the end of embryogenesis: 96% of embryos analyzed reached EgS 9, 87% reached EgS 22, and 71% of embryos hatched as first instar nymphs.

To determine the relationship between the egg stages defined here, and the embryonic stages previously used in the literature (Kainz, 2009; Mito and Noji, 2009), we used epifluorescence to examine either dissected and fixed embryos stained with Hoechst 33342 (EgS 6–18), or undissected embryos through the transparent chorion using a Histone2B-EGFP transgenic cricket line (Nakamura et al., 2010) (EgS 1–5 and 19–24; Figs. 2 and 3). Micrographs of these preparations are grouped into separate figures for different regions of the embryo, including head (Fig. 5), thoracic appendages (Fig. 6), thoracic midline and neuroectoderm (Fig. 7), abdomen (Fig. 8), and posterior abdomen (Fig. 9). Finally, we used optical sections to illustrate the anatomical relationship of mesoderm to ectoderm at the early germ band stage (Fig. 10).

For each egg stage, we provide the following information below: the distinguishing attributes of the egg stage, the age range when the egg stage was observed, and the embryonic stages that

correspond to that period of development. We also describe the major morphogenetic events of development, referencing the staged micrographs included with this paper or directing the reader to existing literature where these morphogenetic processes have been described in additional detail.

The time ranges given below represent the full extent of ages at which an egg stage was observed, rather than the amount of time an egg will spend at a given egg stage. An egg stage's range typically overlapped with those of several other egg stages, as illustrated in Figs. 2, 3 and S1. All descriptions are based on embryonic development at 29 °C (with short periodic transfers to 25 °C for imaging, as described in Section Materials and methods). *G. bimaculatus* embryos can be raised successfully at other temperatures, and the EgS and ES stages can still be used, but the specific times and durations of each developmental event will vary depending on the rearing temperature. We also recorded two time-lapse movies of developing cricket embryos (Movies S1 and S2). These are annotated to highlight the visible characteristics that we use to determine an embryo's egg stage. For EgS 1–17, below we have included the elapsed time range when each egg stage is visible in a supplemental movie. *Note:*

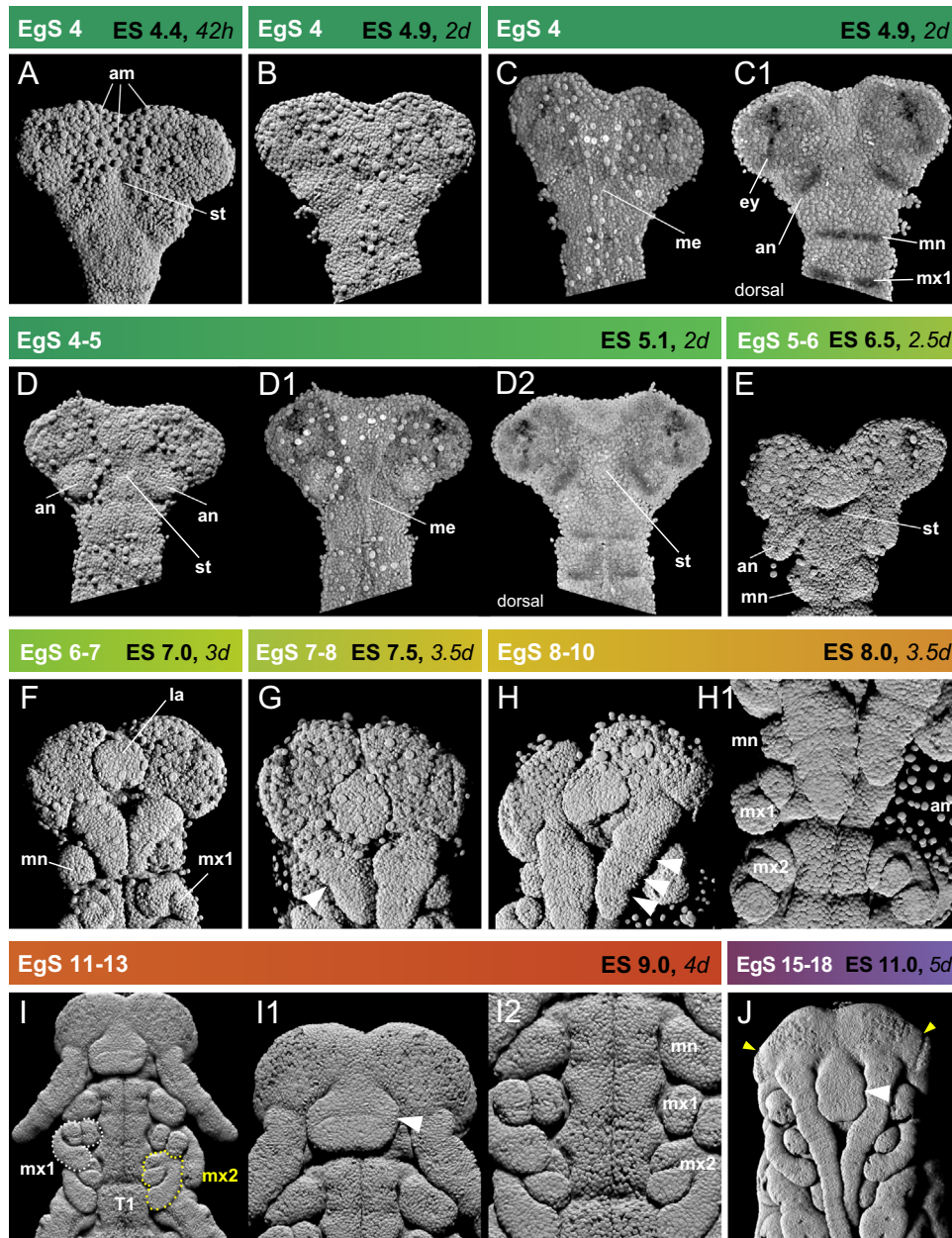


Fig. 5. External morphology of early head and gnathal segment development in *G. bimaculatus*. 3D reconstructions of all nuclei in the anterior of embryos stained with the nuclear dye Hoechst 33342, showing the development of the external head morphologies. Images were rendered in 3D as if illuminated from above by a virtual light source for all panels except for C, C1, D1, and D2, which were rendered as if illuminated from the rear by a virtual light source (see Section [Materials and Methods](#) for details). Embryos are oriented with the ventral side facing up except where noted otherwise. In situ hybridization for *wingless* was also performed on some of these embryos; in those cases, the expression stripes are visible as dark bands perpendicular to the anteroposterior axis in some panels (e.g. C1 and D2). The egg stage (EgS), embryo stage (ES) and age of collection in hours (h) (± 1.5 h) or days (d) (± 1.5 d) after egg laying of the embryos shown is indicated. Embryos were raised at 29 °C.

because these movies were taken in an ambient temperature of 25 °C, the time ranges in the movies do not precisely match the time ranges determined from the snapshots of eggs aged at 29 °C.

Eg1–3: Beginning of embryogenesis through germ band formation

Egg Stage 1: Meiosis and early syncytial cleavages (0–6 h AEL; ES 1.0–1.4; Movie S1 0 d 00:00 h–0 d 09:55 h)

Stage identifiers: Freshly laid egg. The anterior pole is slightly pointed, while the posterior pole is more rounded. The yolk is fine and granular.

Developmental features: A freshly laid cricket egg measures 2.5–3.0 mm along the anteroposterior axis and 0.5–0.7 mm across its width. The egg curves slightly: it is concave on the dorsal side and convex on the ventral side. Note that “dorsal” and “ventral” are defined here based on the future orientation of the embryo inside the egg just before hatching. There is a column of optically dense yolk 60% from the anterior pole of the egg. The female pronucleus is initially located in this column, towards the dorsal side of the egg (Sarashina et al., 2005). The last meiotic divisions occur at ~ 1.5 h AEL and the first mitotic division of the diploid zygotic nucleus is at ~ 3 h AEL (Sato and Tanaka-Sato, 2002). A series of synchronous syncytial nuclear divisions follows and the nuclei gradually move towards the surface of the egg.

Egg Stage 2: Syncytial blastoderm (6–18 h AEL; ES 1.5; Movie S1 0 d 10:00 h–0 d 15:15 h)

Stage identifiers: Energids are visible all over the egg as light-colored dots.

Developmental features: Syncytial divisions continue, and the energids migrate to the surface by 12 h AEL and cellularize from 14 to 16 h AEL (Nakamura et al., 2010; Sarashina et al., 2005). By 18 h AEL there are ~2000 cells uniformly distributed across the surface of the blastoderm; these cells are now dividing asynchronously (Sarashina et al., 2005).

Egg Stage 3: Embryonic rudiment formation (12–36 h AEL; ES 1.6–4.0; Movie S1 0 d 15:20 h–1 d 23:00 h)

Stage identifiers: Cells are no longer obviously visible. The yolk is slightly coarser than that of freshly laid eggs.

Developmental features: At 20 h AEL the embryonic rudiment begins to form as two bilateral aggregations of cells at the ventral posterior region of the egg (Nakamura et al., 2010). At 26 h AEL these aggregations of cells begin to move ventrally, completely fusing at the ventral midline to form a butterfly-shaped embryonic rudiment by 36 h AEL (Miyawaki et al., 2004). The rest of the cells on the yolk's surface appear to become polyploid, as judged by

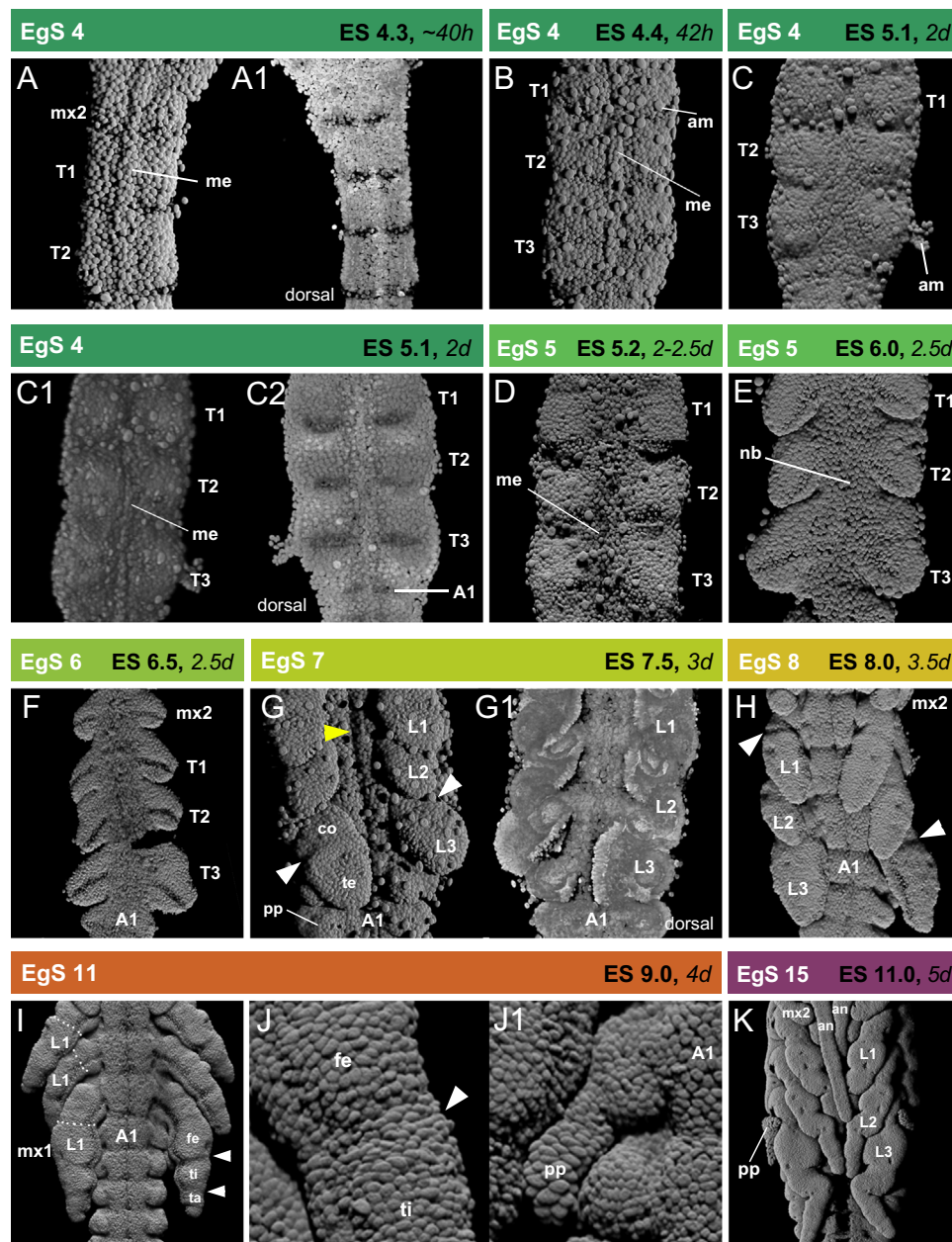


Fig. 6. Thoracic appendage development – external morphology, internal coelomic pouch morphogenesis. 3D reconstructions of all nuclei in the thoracic region of embryos stained with the nuclear dye Hoechst 33342, showing the development of the thorax and thoracic appendages. Images were rendered in 3D as if illuminated from above by a virtual light source for all panels except for A1, C2, and G1, which were rendered as if illuminated from the rear by a virtual light source (see Section **Materials and Methods** for details). Embryos are oriented with the ventral side facing up except where noted otherwise. In situ hybridization for *wingless* was also performed on these embryos; in these cases, the expression stripes are visible as dark bands perpendicular to the anteroposterior axis in some panels (e.g. A1, C2, and F). The egg stage (EgS), embryo stage (ES), and age of collection in hours (h) (± 1.5 h) or days (d) (± 1.5 d) after egg laying of the embryos shown is indicated. Embryos were raised at 29 °C.

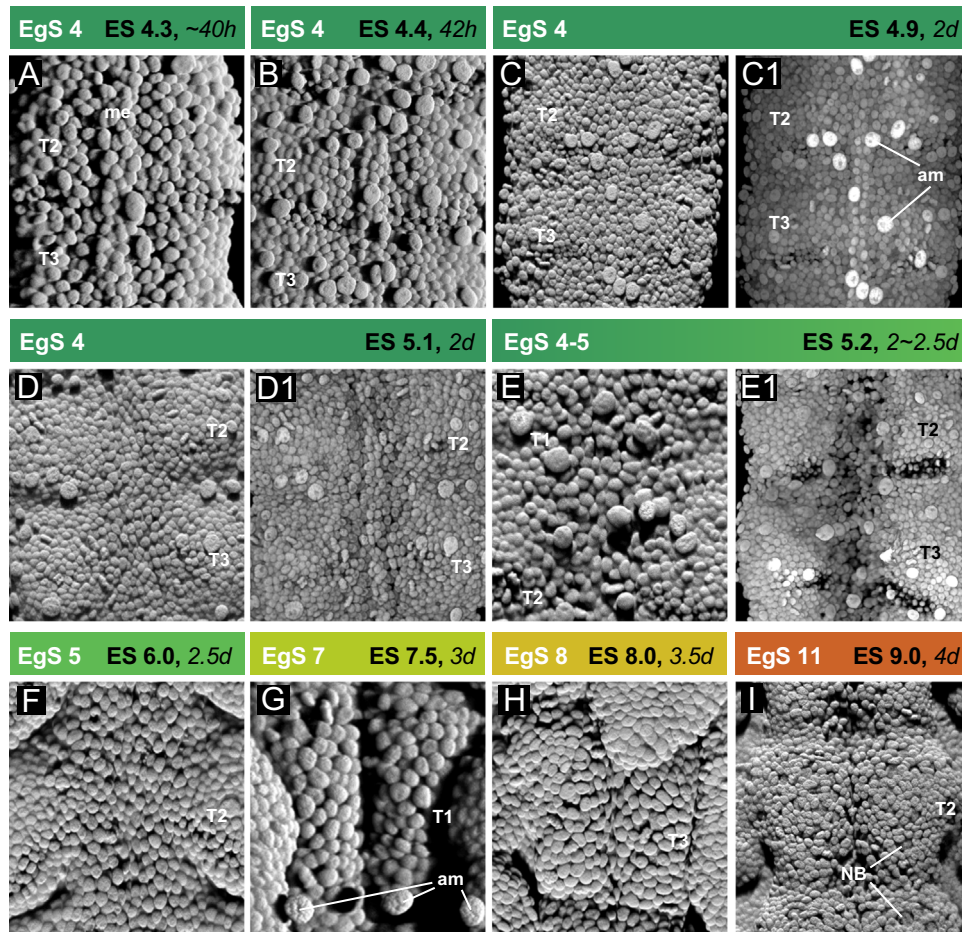


Fig. 7. Thoracic neuroectoderm development – external and internal morphology. 3D reconstructions of all nuclei in one or two thoracic segments of embryos stained with the nuclear dye Hoechst 33342, showing the development of the thoracic ventral midline, neuroectoderm, thoracic neuromeres and neuroblasts. Images were rendered in 3D as if illuminated from above by a virtual light source for all panels except for C1 and E1, which were rendered as if illuminated from the rear by a virtual light source (see Section **Materials and Methods** for details). In situ hybridization for *wingless* was also performed on some of these embryos; in these cases, the expression stripes are visible as dark bands perpendicular to the anteroposterior axis in some panels (e.g. E1). The egg stage (EgS), embryo stage (ES) and age of collection in hours (h) (± 1.5 h) or days (d) (± 1.5 h) after egg laying of the embryos shown is indicated. Embryos were raised at 29 °C.

their enlarged nuclei, and will give rise to both of the extra-embryonic tissues (Nakamura et al., 2010). The amnion appears to form from those extraembryonic cells closest to the embryonic rudiment, which migrate over the rudiment on the ventral side, forming a continuous sheet of cells on the ventral side of the embryo. The serosa forms from the remaining extraembryonic cells, and becomes a continuous sheet of cells attached to the embryo around its circumference, extending dorsally and enveloping the yolk and the dorsal side of the embryo.

The embryonic rudiment then becomes more defined in shape and takes on the shape of an early germ band stage that is typical of most insects: the anterior portion of the germ band (procephalon) is composed of bilateral lobes that will give rise to the head. The rest of the embryo (protocorm) is longer than it is wide, and it will give rise to the thorax and abdomen. In situ hybridization against the cricket orthologs of *wingless* and *hedgehog* has suggested that all head segments and thoracic segments T1 and T2 have been specified by 36 h AEL (Miyawaki et al., 2004). At this point, the abdomen is an unsegmented tissue at the posterior end of the protocorm. This tissue will simultaneously undergo anteroposterior axis elongation and segmentation, giving rise to a total of ten abdominal segments (Kainz et al., 2011; Mito et al., 2011).

To our knowledge, gastrulation has not yet been directly observed in *G. bimaculatus*. However, based on comparative orthopteran embryology, it likely begins during or immediately following the fusion of the bilateral rudiment Anlagen that gives

rise to the single condensed embryonic rudiment (Roonwal, 1936). Cells are thought to delaminate dorsally from the germ band, forming a second layer of cells with distinctly larger nuclei than the cells remaining in the ventral layer. The dorsal cell layer likely gives rise to the mesendoderm, while the ventral layer acquires ectodermal fate, including the neuroectoderm along the ventral midline.

EgS 4–6: Abdomen segmentation and beginning of anatrepsis

Egg Stage 4: Early germ band (36–54 h AEL; ES 4.0–5.2; Movie S1 1 d 23:05 h–2 d 12:10 h)

Stage identifiers: Yolk has just begun to separate into small fragments. The yolk is often absent from one or both ends of the eggshell. The elongating germ band is visible at the posterior end of the egg.

Developmental features: The T3 segment has formed by 39 h AEL (Miyawaki et al., 2004). After the first ~ 2 d of embryogenesis, embryos at the same age begin to slightly diverge in the extent of their developmental progress. Thus, for events after 2 d AEL, we refer to embryonic stages rather than time AEL in the subsequent text descriptions. By approximately 2 d AEL, mesodermal cells have formed along the entire anterior–posterior axis (Fig. 10). By ES 4.9, the amnion has covered the ventral surface of the newly formed germ band. In Hoechst 33342-stained embryos, amniotic

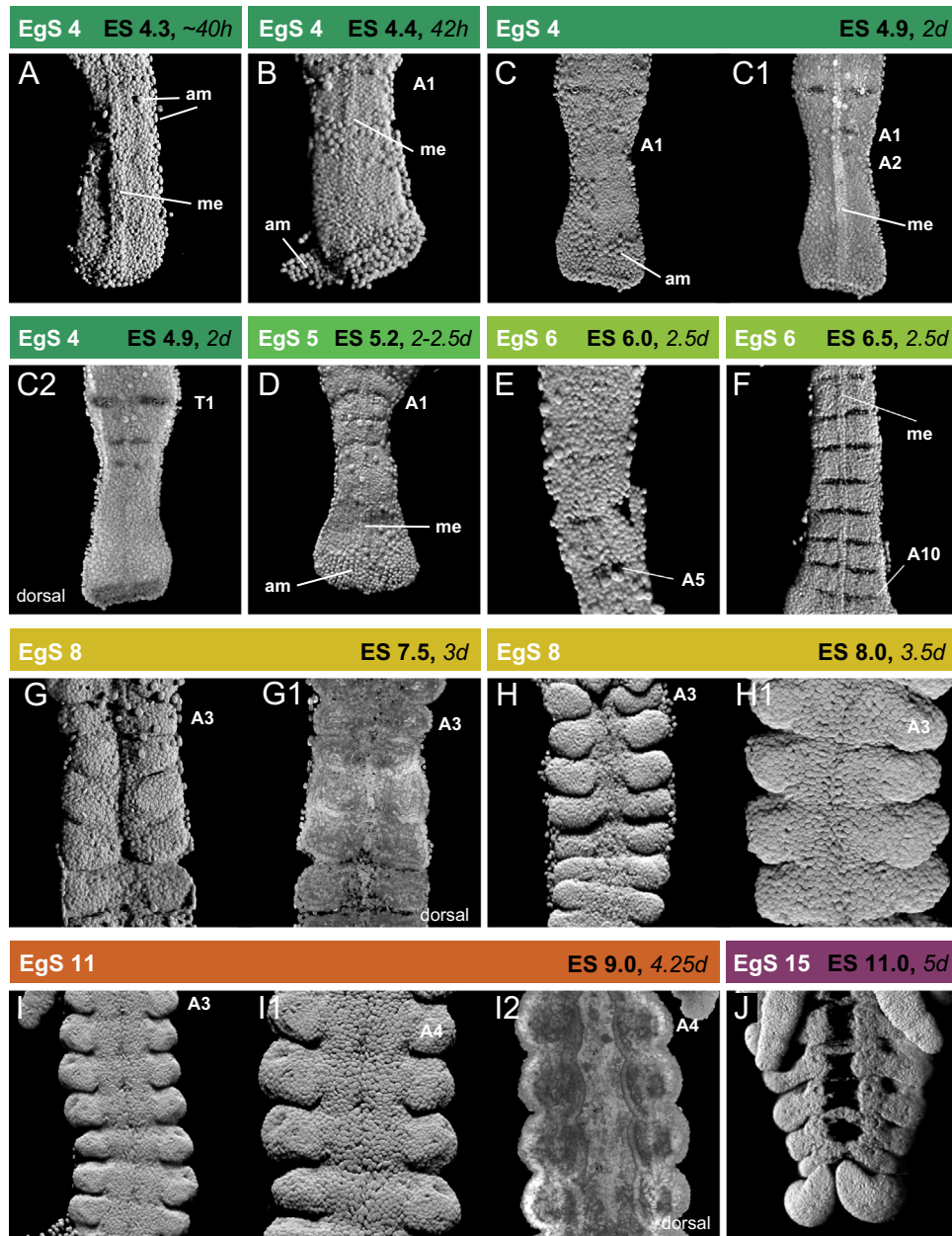


Fig. 8. Anterior abdominal development – progression of segmentation. 3D reconstructions of all nuclei in the anterior abdominal region of embryos stained with the nuclear dye Hoechst 33342, showing the development of segment morphologies. Images were rendered in 3D as if illuminated from above by a virtual light source in all panels except for G1 and I2, which were rendered as if illuminated from the rear by a virtual light source (see Section [Materials and Methods](#) for details). Embryos are oriented with the ventral side facing up except where noted otherwise. In situ hybridization for *wingless* was also performed on some of these embryos; in these cases, the expression stripes are visible as dark bands perpendicular to the anteroposterior axis in some panels (e.g. C2, and F). The egg stage (EgS), embryo stage (ES) and age of collection in hours (h) (± 1.5 h) or days (d) (± 1.5 d) after egg laying of the embryos shown is indicated. Embryos were raised at 29 °C.

cells are visible as large spherical nuclei ventral to the embryo surface (e.g. [Fig. 5A](#) and [B](#)). There is a ridge of mesectodermal cells that runs down the ventral midline of the embryo from the head to the posterior end of the abdomen ([Kainz et al., 2011](#)). This ridge is 2–4 cells wide through the thorax and abdomen ([Fig. 6A](#) and [B](#); [Fig. 7A](#) and [B](#); [Fig. 8A](#) and [B](#)) and it broadens anteriorly to form a rough triangle between the lobes of the head ([Fig. 5C](#)).

At ES 4.9, the two lobes of the head retain a similar overall shape to that of the protocephalon of the newly condensed germ band ([Fig. 5A](#) and [B](#)). Thoracic segments are not morphologically distinct from other segments, and the mesectodermal ridge is still visible ([Fig. 6A](#) and [B](#); [Fig. 7C](#) and [C1](#)). At ES 5.1, the stomodaemum arises at ES 5.1 as a small indentation between the antennal lobes along the ventral midline ([Fig. 5D](#) and [D2](#)) and the presumptive

antennae begin to bulge out ventrally from the posterior lateral region of each head lobe ([Fig. 5D](#) and [D1](#)). Bilateral bulges at the lateral edges of each thoracic segment indicate the first steps of leg Anlagen formation ([Fig. 6C](#), [C1](#) and [C2](#); [Fig. 7D](#) and [D1](#)). At ES 5.2, each thoracic segment is slightly more rounded, and the ridge of mesectoderm is no longer visible ([Fig. 6D](#); [Fig. 7E](#) and [E1](#)).

Abdominal segments form sequentially, from anterior (segment A1) to posterior (segment A10) ([Kainz et al., 2011](#); [Mito et al., 2011](#)). If one uses *wingless* expression stripes as markers for acquisition of segmental identity, segment A1 arises at 42 h AEL, A2 at 44 h AEL, A3 at 46 h AEL, and A4 at 48 h AEL (ES 4.4, 4.9, 5.0, and 5.2, respectively; [Mito and Noji, 2009](#); [Miyawaki et al., 2004](#)). The mesectodermal ridge remains extended along the length

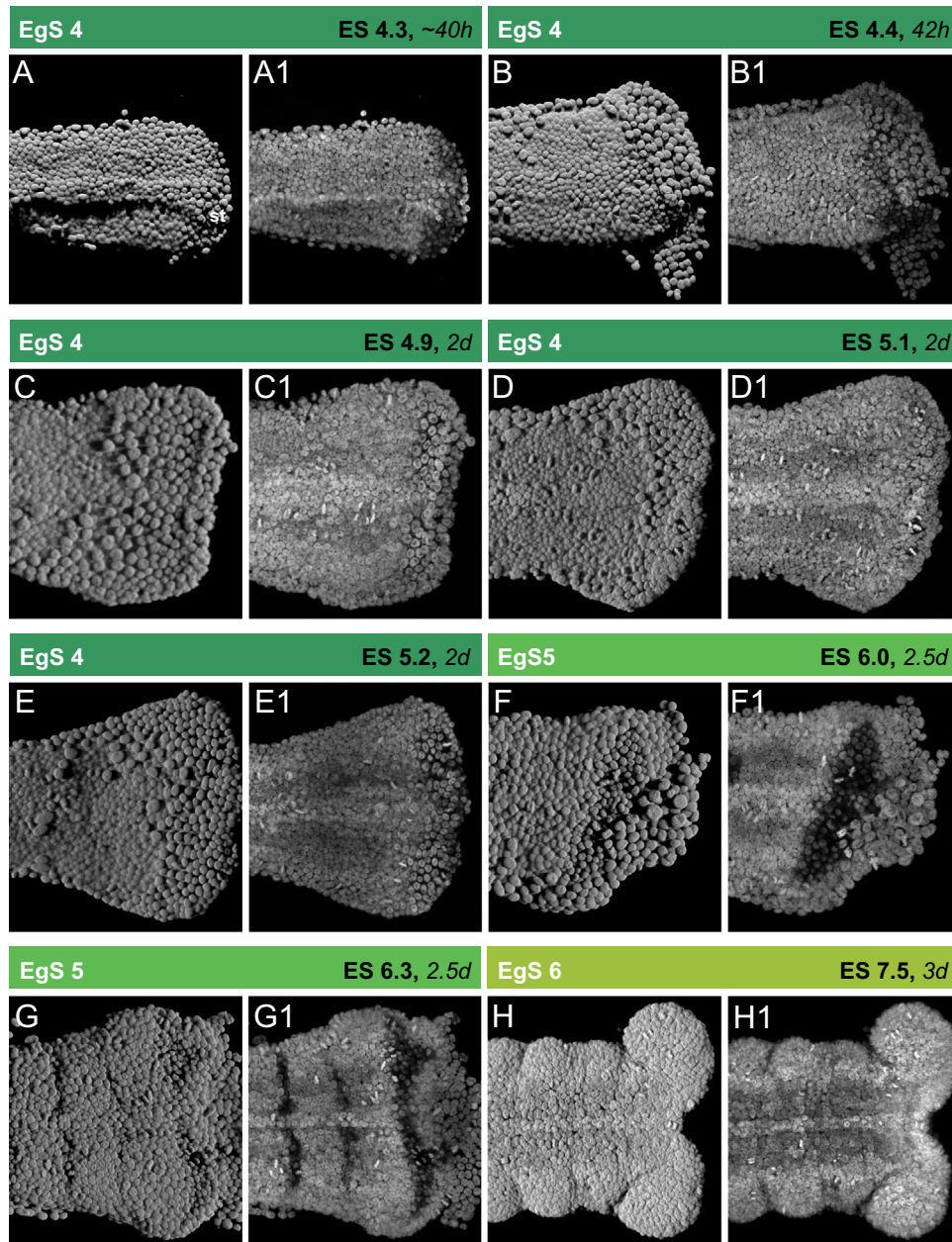


Fig. 9. Posterior abdominal development. 3D reconstructions of all nuclei in the posterior abdominal region of embryos stained with the nuclear dye Hoechst 33342, showing the development of the telson and cerci primordia. Panels A, B, C, D, E, F, G, and H were rendered in 3D as if illuminated from above by a virtual light source; A1, B1, C1, D1, E1, F1, G1, and H1 were rendered as if illuminated from the rear by a virtual light source (see Section [Materials and Methods](#) for details). In situ hybridization for *wingless* was also performed on some of these embryos; in these cases, the expression stripes are visible as dark bands perpendicular to the anteroposterior axis in some panels (e.g. G1). The egg stage (EgS), embryo stage (ES) and age of collection in hours (h) (± 1.5 h) or days (d) (± 1.5 d) after egg laying of the embryos shown is indicated. Embryos were raised at 29 °C.

of the abdomen, lengthening as segments form (Figs. 8C and D, 9A–F1).

Egg Stage 5: Abdomen elongation continues (2.25–2.75 d AEL; ES 5.2–6.5; Movie S1 2 d 12:15 h–3 d 05:35 h)

Stage identifiers: Yolk is now entirely in small fragments, and may be absent from one or both ends of the eggshell. The germ band is now fully submerged in the yolk.

Developmental features: By ES 6.0, the thoracic limb buds have initiated as bulbous swellings that protrude from the lateral edges of each thoracic segment, pointing laterally outward and towards the posterior (Figs. 6E and 7F). The abdomen continues to elongate, with stripes of *wingless* expression arising at the poste-

rior, indicating continued anteroposterior segment generation (Fig. 9G–H1). By ES 6.5, the limbs have elongated, extending along the proximodistal axis (Fig. 6F). Since several recent studies have described limb formation in close detail (reviewed by Nakamura et al. (2008a)), we do not further discuss appendage formation or patterning in depth here.

Egg Stage 6: Anatrepsis begins (2.5–3 h AEL; ES 6.0–7.0; Movie S1 3 d 05:40 h – end of Movie S1 and Movie S2 3 d 00:00 h–3 d 17:15 h)

Stage identifiers: Yolk is in visibly larger fragments than at the previous stage, but the overall egg shape is unchanged. Embryo is only rarely visible through the yolk.

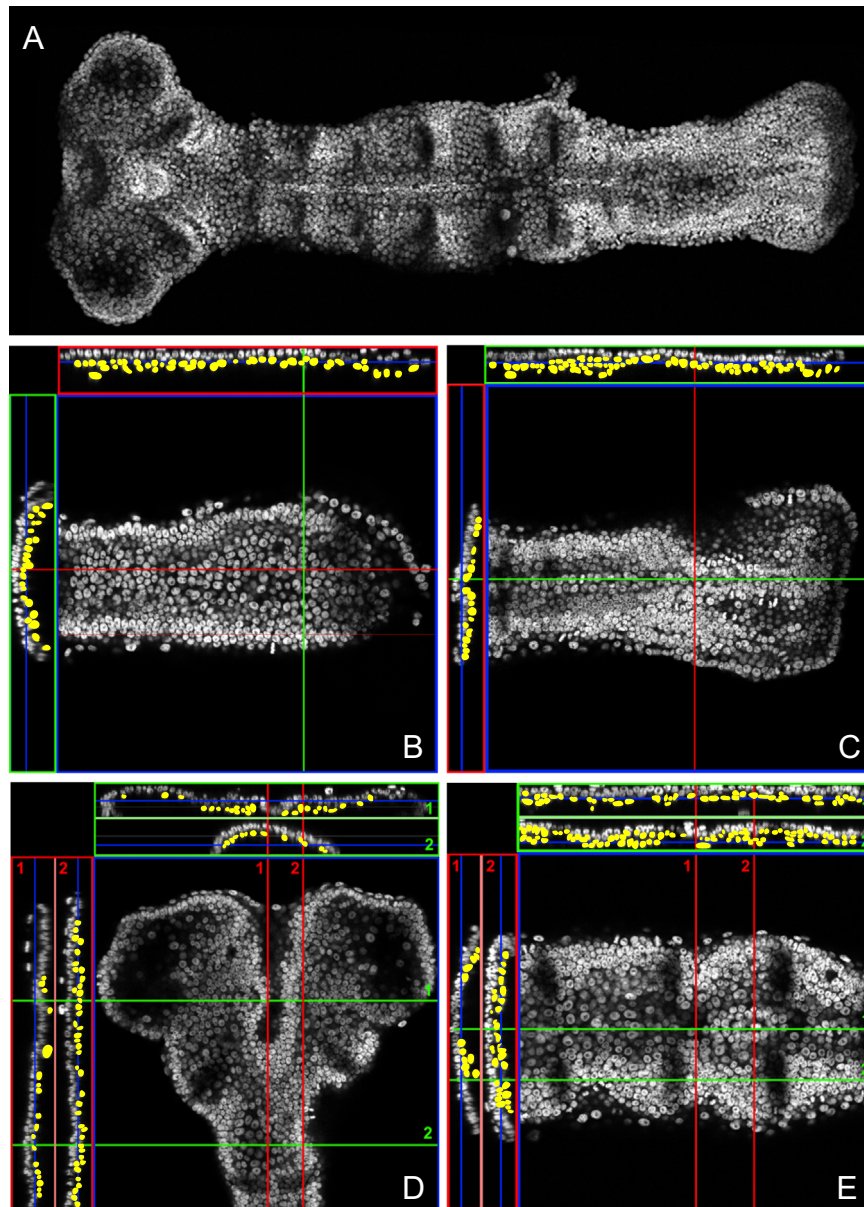


Fig. 10. Mesoderm formation. (A) 2D projection of optical sections through an embryo at EgS 4 (ES 4.9), showing an overview of the entire embryo stained with the nuclear dye Hoechst 33342. In situ hybridization for *wingless* was also performed on these embryos; the expression stripes are visible as dark bands perpendicular to the anteroposterior axis. At this stage, the embryo is bilayered, with a single dorsal layer of mesoderm and a single ventral layer of ectoderm. Panels (B–E) are single optical sections of embryos of the same stage. (B) Single optical section through the dorsal plane of the posterior abdomen, showing a uniform layer of mesodermal cells. Orthogonal projections along the plane of the anterior–posterior axis (top) and proximodistal axis (left) are shown, with mesoderm cells indicated in yellow false coloring. (C) Single optical section through the ventral plane of the posterior abdomen, showing a layer of ectodermal cells, including the mesectoderm along the midline. Orthogonal projections along the plane of the anterior–posterior axis (top) and proximodistal axis (left) are shown, with mesoderm cells indicated in yellow false coloring. (D) Single optical section through the dorsal plane of the head, showing that the head lobes are populated by mesodermal cells. Orthogonal projections along the plane of the anterior–posterior axis (left) and proximodistal axis (top) are shown, with mesoderm cells indicated in yellow false coloring. (E) Single optical section through the dorsal plane of the thorax, showing a uniform layer of mesodermal cells. Orthogonal projections along the plane of the anterior–posterior axis (top) and proximodistal axis (left) are shown, with mesoderm cells indicated in yellow false coloring.

Developmental features: While abdominal elongation and segmentation are occurring, the whole embryo is moving within the yolk in a process called anatrespsis. Over approximately 1.5 d, the embryo shifts posteriorly, following the interior curve of the egg around the posterior, from ventral to dorsal, until the embryo has performed a 180° re-orientation. This can be observed in Movie S1 (2 d 00:00 – end of movie) and the process is even clearer in fixed specimens (Kainz, 2009). At the end of anatrespsis, the anterior end of the embryo faces the posterior of the egg, while the embryo posterior points towards the anterior of the egg.

By ES 6.5, the antennal primordia have formed into conspicuous protruding lobes, and the gnathal segments have formed laterally

rounded bulges that will give rise to the gnathal appendages (Fig. 5E). The antennae and gnathal appendages continue to grow laterally outward through ES 7.0 (Fig. 5F). The stomodaeum deepens by ES 6.5 to become a crescent shaped cleft at the ventral midline (Fig. 5E). This cleft is located immediately posterior to an ovoid ventral protrusion of tissue that will become the labrum (Fig. 5E and F). During germ band elongation (ES 4.4–7.5), the abdomen is a lengthening strip of cells, widening at the posterior terminus to the shape of a tapered spade (Figs. 8A–F and 9A–H). Segments A8–10 form at ES 6.5–7.5 (Fig. 8F) (Kainz, 2009; Mito and Noji, 2009). By ES 7.5 the cerci have emerged as bilateral lobes protruding from the posterior of the abdomen (Fig. 9H and H1).

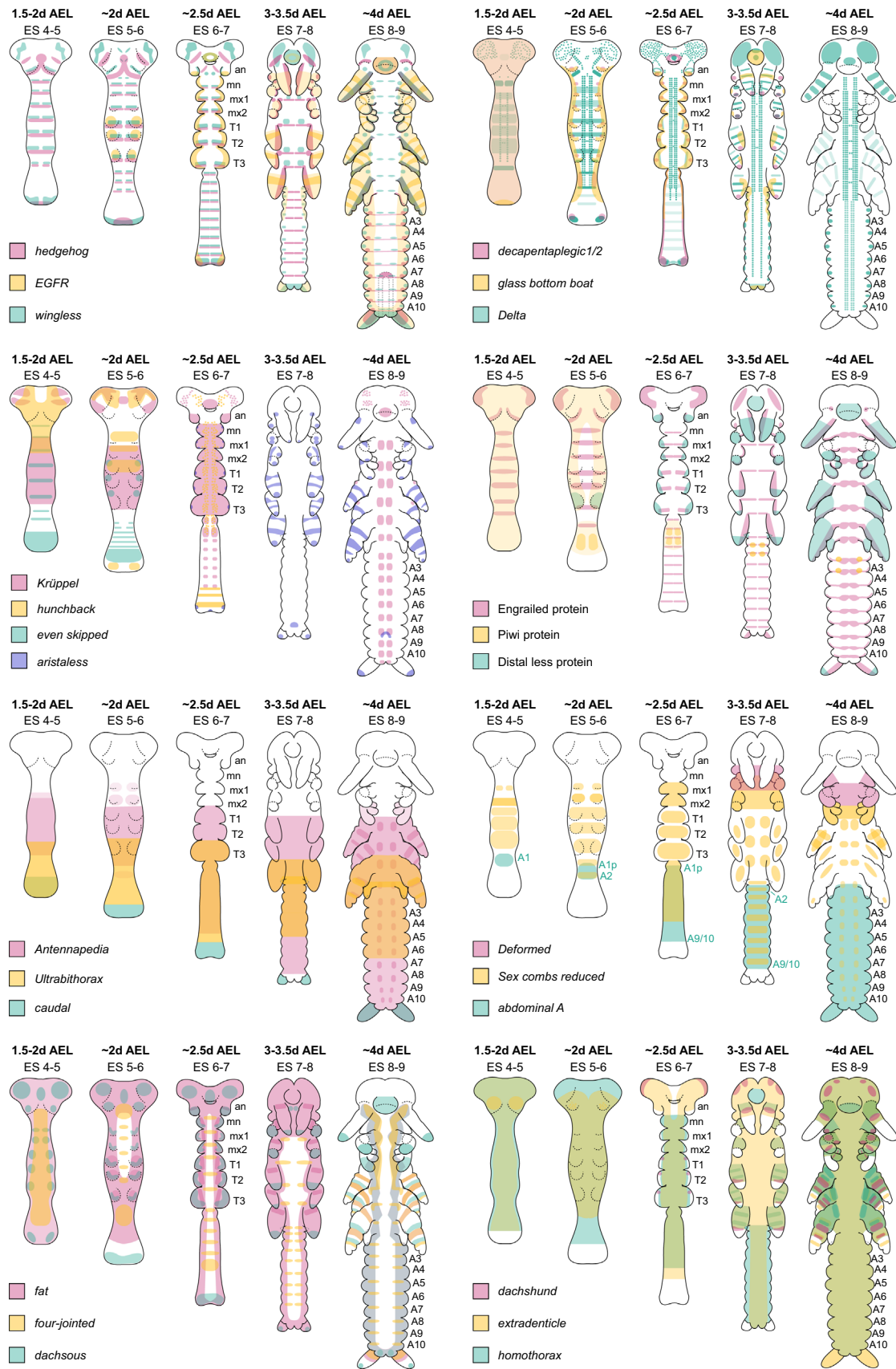


Fig. 11. Gene expression through development. Schematics of the expression patterns of various developmental genes throughout the mid-embryonic stages when much of the major pattern formation takes place (ES 4–9, corresponding to EgS 4–13). The shading of a color represents differences in expression intensity. For example, *EGFR* expression in 4 d AEL embryos is detectable throughout the limbs, but it is expressed at higher levels in bands perpendicular to the proximodistal axis of each limb (Nakamura et al., 2008b). Data were collated from the literature as follows: *hedgehog* (Miyawaki et al., 2004; Niwa et al., 2000); *EGFR* (Nakamura et al., 2008b); *wingless* (Kainz et al., 2011; Miyawaki et al., 2004; Niwa et al., 2000); *decapentaplegic*: data shown for 1.5–3.5 d AEL (Donoughe et al., 2014; Niwa et al., 2000); *glass bottom boat* (Donoughe et al., 2014); *Delta* (Kainz et al., 2011; Mito et al., 2006); *Krüppel* (Inoue et al., 2004; Mito et al., 2006); *hunchback*: data shown for 1.5–2.5 d AEL (Inoue et al., 2004; Mito et al., 2005); *even-skipped*: data shown for 1.5–2 d AEL (Mito et al., 2007); *aristales*: data shown for 2.5–4 d AEL (Miyawaki et al., 2002); *Engrailed* (Niwa et al., 1997); *Piwi* (Ewen-Campen et al., 2013); *Distalless* (Inoue et al., 2002; Niwa et al., 1997); *Antennapedia*, *Ultrabithorax*, *Sex combs reduced* and *abdominal-A* (Zhang et al., 2005); *caudal* (Shinmyo et al., 2005); *Deformed*: data shown for 3–4 d AEL (Mito et al., 2006, 2008); *fat*, *four-jointed* and *dachsous* (Bando et al., 2009); *dachshund*: data shown for head and appendages for 2.5–4 d AEL (Inoue et al., 2004, 2002); *extradenticle* (Inoue et al., 2002; Mito et al., 2008); and *homothorax* (Inoue et al., 2002; Ronco et al., 2008).

EgS 7–9: End of anatrepsis and appendage elongation

Egg Stage 7: Egg expansion begins (3–3.5 d AEL; ES 7.0–7.5; Movie S2 3 d 14:15 h–4 d 02:25 h)

Stage identifiers: Large yolk fragments are beginning to break up. Egg length is the same as in the previous stages, but egg girth has increased slightly. The egg is no longer bowed and it tapers a little more sharply than before at the ends.

Developmental features: At this stage of embryogenesis, overall egg shape and size become useful for staging. We used an ImageJ macro to automatically extract egg shape measurements from 42 eggs at 37 different time points (Supplementary Fig. S2). This revealed that most egg shape change occurs from approximately 3 to 4 d AEL. Because automated analysis did not always accurately capture egg outlines, we selected ten individuals that were imaged every 6-hours and that survived through to hatching, for manual verification of egg measurements. We manually measured each egg at multiple time points throughout embryogenesis, with closely spaced time points around the 3–4 d AEL period. This revealed that egg width and length increase sharply from 3 to 3.5 d AEL, then continue to increase, albeit, less dramatically, from 3.5 to 4 d AEL (Fig. 4A–C). Egg volume roughly doubles from 3 to 4 d AEL (Fig. 4D). Egg aspect ratio slowly changes during embryogenesis, beginning at a length to width ratio of 5, and ending at a ratio of 4.2 (Fig. 4E). This is qualitatively similar to the egg enlargement described for the cricket *Telogyllus emma*, in which a 35% increase in egg width was observed at from 4 to 5 d AEL when *T. emma* was raised at 30 °C (Masaki, 1960).

Egg Stage 8: Egg expansion continues (3.25–4 d AEL; ES 7.2–8.0; Movie S2 4 d 01:45 h–4 d 10:00 h)

Stage identifiers: Egg is becoming longer, wider, and tauter. The egg is more bulbous at the posterior than at EgS 7, and more tapered at the anterior than EgS 9.

Developmental features: By ES 7.5, the antennae and gnathal appendages have continued to elongate and the antennae have one constriction at half of their length (Fig. 5G). A groove has formed at the ventral midline of the thorax in the former location of the mesectoderm (Figs. 6G and 7G). The limbs have begun to constrict at their midpoint, separating the more proximal coxopodite from the distal telopodite (Fig. 6G and G1). This constriction will mark the boundary between the trochanter and femur (Miyawaki et al., 2002). The pleuropodia, which are transient appendages on the A1 segment that are resorbed before hatching, have begun to grow laterally (Fig. 6G). Each abdominal segment becomes gently rounded laterally in two bilateral bulges (Fig. 8G). Optical sections through these bulges show that a coelomic pouch is forming from the mesoderm within each of these incipient abdominal segment lobes (Fig. 8G1).

Egg Stage 9: Anatrepsis completion (3.75–4.5 d AEL; ES 7.5–8.5; Movie S2 4 d 07:45 h–4 d 14:05 h)

Stage identifiers: Egg is at its largest and tautest. The anterior end is now a smooth hemispherical curve. Yolk has not begun to clear from the area dorsal to the head.

Developmental features: At ES 8.0, the antennae have three constrictions and the maxillary appendages have begun to form lobes that will give rise to palps and other maxillary mouthparts (Fig. 5H and H1) (Miyawaki et al., 2002). Additional grooves now run perpendicular to the ventral midline in the thorax, creating morphological separation between thoracic segments (Figs. 6H and 7H). The first limb constriction on each thoracic limb deepens as the telopodite

elongates (Fig. 6H). The lateral lobes of the abdominal segments protrude ventrally with furrows perpendicular to the anteroposterior axis separating adjacent lobes and creating clear morphological demarcation of each abdominal segment (Fig. 8H). A ventral midline groove, a posterior continuation of the thoracic ventral midline groove, is now visible on the abdomen (Fig. 8H1).

EgS 10–12: Appendage segmentation

Egg Stage 10: Yolk begins clearing dorsal to embryonic head (4–5 d AEL; ES 8.0–8.7; Movie S2 4 d 14:10 h–4 d 23:20 h)

Stage identifiers: Yolk begins to clear away from the space that is dorsal to the embryo's head. This is most easily visible when the egg is viewed laterally.

Egg Stage 11: Yolk clearing complete in embryonic head region (4.25–5.5 d AEL; ES 8.5–9.0; Movie S2 4 d 23:025 h–5 d 12:55 h)

Stage identifiers: Yolk has completely cleared dorsal to the head. This is often visible as a transparent notch in the yolk when viewed laterally. The yolk has not yet begun to pull away from the posterior end of the egg.

Developmental features: By ES 9.0, the antennae and gnathal appendages have elongated further, and now both pairs of maxillary appendages are trilobed (Fig. 5I and I2). The labrum is creased across its width perpendicular to the anteroposterior axis (Fig. 5I1). The telopodite of each limb has acquired at least one additional constriction, separating the femur from the tibia. A more distal constriction may also be visible in some limbs; this will be the boundary between the tibia and tarsus (Fig. 6I and J). The pleuropodia have grown laterally and posteriorly so that they lie lateral to the A2 segment (Fig. 6J1). The thoracic neuromeres, visible as bilateral ventral bulges of the thoracic segments, are more clearly defined (Fig. 7I). The furrows separating the lateral abdominal lobes from each other have deepened slightly (Fig. 8I–I1). The medial margin of the coelomic pouches is clearly defined into a rounded surface that bulges in each hemisegment towards the midline of the embryo (Fig. 8I and I2).

Egg Stage 12: Yolk clearing begins at egg posterior (5–5.75 d AEL; ES 8.7–9.5; Movie S2 5 d 13:00 h – 6 d 11:50 h)

Stage identifiers: Yolk begins to pull away from the posterior end of the egg to form a gap. Yolk is absent in the space dorsal to the embryo's head.

EgS 13–15: Katatrepsis

Egg Stage 13: Katatrepsis begins (5.25–6 d AEL; ES 9.0–9.9; Movie S2 6 d 02:35 h–6 d 06:00 h and 6 d 11:55–6 d 22:45 h)

Stage identifiers: The cleared notch in the yolk is fully connected with the yolk-free space created at the posterior end of the egg, as the head emerges posteriorly from the yolk. None of the gnathal appendages are yet free from the yolk.

Developmental features: Immediately before the onset of katatrepsis, the yolk and the embryo roll 60–90° within the eggshell around an imaginary line drawn from the anterior to the posterior tip of the egg (Movie S2, 6 d 00:00 h–6 d 03:55 h and 6 d 16:45 h–6 d 21:35 h). During katatrepsis, the head of the embryo, having emerged posteriorly from the yolk, will move along the ventral side of the egg towards the anterior pole of the egg, resulting in a reorientation of the

anteroposterior axis of the embryo with respect to that of the egg, essentially reversing the movement of anatrepsis.

Egg Stage 14: Midway point of katatrepsis (5.25–6.5 d AEL; ES 10.0; Movie S2 6 d 06:05 h–6 d 13:55 h and 6 d 22:50 h–7 d 00:50 h)

Stage identifiers: The midway point of katatrepsis. The head of the embryo is located approximately one-third of the egg length away from the posterior pole, lying almost exactly immediately ventrally to the posteriormost extent of the embryo posterior, which is still lying on the dorsal side of the eggs. The thoracic appendages are exposed in the yolkless space in the posterior of the egg.

Egg Stage 15: Katatrepsis has completed (5.25–6.5 d AEL; ES 11.0; Movie S2 6 d 14:00 h–7 d 13:10 h)

Stage identifiers: Katatrepsis is complete, with the head now pointing towards the anterior of the egg. A portion of the yolk forms a broad patch on the dorsal side of the embryo, but the majority of the yolk mass is anterior to the embryo. When viewed ventrally, 55–60% of the egg is taken up by the embryo.

Developmental features: The duration of katatrepsis is somewhat variable. For example, Movie S2 shows two embryos that were laid within 60 min of each other. Counting from when a cricket's head first emerged into the posterior yolk-free space to when the embryo completely straightened out along the AP axis, katatrepsis lasted 4 h 30 min in the top embryo and 2 h 55 min in the bottom embryo.

By ES 11.0, the antennae and gnathal appendages have elongated and now point posteriorly on the ventral side of the embryo (Fig. 5J). What began as a slight crease perpendicular to the anteroposterior axis of the labrum has become a deeper constriction that divides the labrum into an anterior and a posterior region (Fig. 5J). The thoracic limbs have elongated and they lie along the ventral face of the embryo, with each limb segment morphologically distinct (Fig. 6K). The anteriormost abdominal segments have broadened laterally, which results in an abdomen that is wedge-shaped, tapering toward the posterior (Fig. 8J). The furrows between the lateral abdominal lobes and abdominal segments have deepened further, and now the cerci have elongated and curled anteriorly around the ventral tip of the abdomen (Fig. 8J).

EgS 16–24: Dorsal closure through hatching

Egg Stage 16: Dorsal closure (5.75–7.75 d; ES 11; Movie S2 7 d 11:15 h–8 d 14:00 h)

Stage identifiers: The dorsal patch of yolk narrows as dorsal closure begins. Dorsal closure proceeds from posterior to anterior. When viewed ventrally, 65–70% of the egg is taken up by the embryo. Eyes are lightly pigmented.

Egg Stage 17: Dorsal closure ongoing, eyes more darkly pigmented (7–8.75 d AEL; ES 11.0–12.0; Movie S2 8 d 03:30 h – end of Movie S2)

Stage identifiers: A bulge of yolk remains anterior to the embryo, but is reduced relative to previous stages as this anterior yolk mass is taken up into the gut as dorsal closure proceeds. When viewed ventrally, 80–85% of the egg is taken up by the embryo. Dorsal closure is well advanced in the abdomen. Eyes are more darkly pigmented.

Egg Stage 18: Anterior yolk margin level with eyes (7–9.25 d AEL; ES 11.0–12.0)

Stage identifiers: The anterior yolk mass has been taken up into the gut to the extent that its anteriormost extent is now slightly posterior to the anterior tip of the head. A yolk-free gap exists between the anterior of the embryo and the anterior eggshell.

Egg Stage 19: Yolk fully enclosed posterior to head (7.5–9.75 d AEL; ES 12.0–13.0)

Stage identifiers: The yolk is entirely enclosed within the gut posterior to the head, and dorsal closure is completed. The yolk-free gap remains between the anterior of the embryo and the eggshell. This gap is about the same size as in the previous stage.

Egg Stage 20: Anterior gap closure begins (8.5–10.25 d AEL; ES 12.0–14.0)

Stage identifiers: Embryo begins to move towards the anterior of the egg, so that the yolk-free gap anterior to the embryo becomes reduced to approximately half the size of that in the previous stage.

Egg Stage 21: Cuticle pigmentation begins (9–11.25 d AEL; ES 13.0–14.0)

Stage identifiers: Only a very small yolk-free gap remains anterior to the embryo. Eyes are larger and darker. Pigment is now visible in the cuticle in other parts of the body, particularly the cerci.

Egg Stage 22: Anterior gap closure complete (10–12 d AEL; ES 14.0)

Stage identifiers: No yolk-free gap remains anterior to the embryo.

Egg Stage 23: Chaetae pigmentation visible (11.5–14 d AEL; ES 15.0)

Stage identifiers: Embryo appears to have expanded, filling the volume of the eggshell completely. Cuticle is darker all over. Bristles are visible on legs, antennae, and on the dorsal side of the body.

Egg Stage 24: Pre-hatching to hatching (12–14 d AEL; ES 16.0)

Stage identifiers: Embryo hatches.

Developmental features: The embryo hatches as a first instar nymph with a body plan and overall appearance much like that of an adult, but lacking conspicuous wings or ovipositor. First instar hatchlings are initially lightly pigmented, but darken during the first day following hatching. Over the next five weeks, the nymph will molt eight times, emerging approximately seven weeks AEL as a sexually mature adult.

To complement the 3D reconstructions of early embryos (Figs. 5–9), we wished to facilitate developmental studies in *G. bimaculatus* by summarizing the dynamics of a number of molecular markers relevant to developmental patterning. To this end, we schematized a set of previously published gene expression patterns (Fig. 11). We consolidated these data because for several of the genes, different aspects of the expression pattern (e.g. in different embryonic regions, or at different developmental stages) have been described in fragmented ways scattered across multiple publications. We focused on essential, highly conserved developmental genes, omitting those that were expressed ubiquitously or in patterns that were described as similar to other included genes. We chose 25 genes that have distinct expression patterns in the early cricket embryo, and whose orthologs identify specific tissue fates or spatial domains in the embryos of many

different animal species. These expression patterns can be used to diagnose defects in loss of function conditions (see e.g. Mito et al. (2008)), or to precisely determine the extent of developmental progress (see e.g. Kainz et al. (2011)). In addition, these molecular markers are helpful for generating hypotheses about which cell signaling pathways could be acting to specify a tissue of interest (see e.g. Donoughe et al. (2014)). More broadly, these expression patterns can be used as molecular evidence to support or undermine conjectures about arthropod developmental homology.

Acknowledgments

Thanks to Franz Kainz for preparing some of the embryos used in the analysis, Sam Kunes (Harvard University, MA, USA) and Greg Davis (Bryn Mawr College, PA, USA) for antibody reagents, Taro Nakamura for the image of a cricket hatchling, and the Extavour lab for discussion of the results and comments on the manuscript. This work was supported by National Science Foundation (NSF) Grant IOS-1257217 to CGE and an NSF predoctoral fellowship to SD.

Appendix A. Supplementary material

Supplementary data associated with this article can be found in the online version at <http://dx.doi.org/10.1016/j.ydbio.2015.04.009>.

References

- Bando, T., Ishimaru, Y., Kida, T., Hamada, Y., Matsuoka, Y., Nakamura, T., Ohuchi, H., Noji, S., Mito, T., 2013. Analysis of RNA-seq data reveals involvement of JAK/STAT signalling during leg regeneration in the cricket *Gryllus bimaculatus*. *Development* 140, 959–964.
- Bando, T., Mito, T., Maeda, Y., Nakamura, T., Ito, F., Watanabe, T., Ohuchi, H., Noji, S., 2009. Regulation of leg size and shape by the Dachshund/Fat signalling pathway during regeneration. *Development* 136, 2235–2245.
- Bentley, D., Keshishian, H., Shankland, M., Torioian-Raymond, A., 1979. Quantitative staging of embryonic development of the grasshopper, *Schistocerca nitens*. *J. Embryol. Exp. Morphol.* 54, 47–74.
- Büning, J., 1994. *The Insect Ovary: Ultrastructure, Previtellogenic Growth and Evolution*. Chapman and Hall, London.
- Chapman, R.F., Whitham, F., 1968. The external morphogenesis of grasshopper embryos. *Proc. R. Entomol. Soc. Lond.* 43, 161–169.
- Donoughe, S., Nakamura, T., Ewen-Campen, B., Green II, A.D., Henderson, L., Extavour, C.G., 2014. BMP signaling is required for the generation of primordial germ cells in an insect. *Proc. Natl. Acad. Sci. USA* 111, 4133–4138.
- Ewen-Campen, B., Donoughe, S., Clarke, D.N., Extavour, C.G., 2013. Germ cell specification requires zygotic mechanisms rather than germ plasm in a basally branching insect. *Curr. Biol.* 23, 835–842.
- Ewen-Campen, B., Srouji, J.R., Schwager, E.E., Extavour, C.G., 2012. *oskar* predates the evolution of germ plasm in insects. *Curr. Biol.* 22, 2278–2283.
- Hägele, B.F., Wang, F.-H., Sehnaal, F., Simpson, S.J., 2004. Effects of crowding, isolation, and transfer from isolation to crowding on total ecdysteroid content of eggs in *Schistocerca gregaria*. *J. Insect Physiol.* 50, 621–628.
- Harrat, A., Petit, D., 2009. Chronology of embryonic development of the strain “Espiguette” with or without diapause in *Locusta migratoria* Linnaeus (Orthoptera: Acrididae). *C. R. Biol.* 332, 613–622.
- Inoue, Y., Miyawaki, K., Terasawa, T., Matsushima, K., Shinmyo, Y., Niwa, N., Mito, T., Ohuchi, H., Noji, S., 2004. Expression patterns of dachshund during head development of *Gryllus bimaculatus* (cricket). *Gene Expr. Patterns* 4, 725–731.
- Inoue, Y., Niwa, N., Mito, T., Ohuchi, H., Yoshioka, H., Noji, S., 2002. Expression patterns of *hedgehog*, *wingless*, and *decapentaplegic* during gut formation of *Gryllus bimaculatus* (cricket). *Mech. Dev.* 110, 245–248.
- Kainz, F., 2009. *Cell Communication During Patterning: Notch and FGF Signalling in Gryllus bimaculatus and Their Role in Segmentation*, Department of Zoology, University of Cambridge, Cambridge, p. 161.
- Kainz, F., Ewen-Campen, B., Akam, M., Extavour, C.G., 2011. Delta/Notch signalling is not required for segment generation in the basally branching insect *Gryllus bimaculatus*. *Development* 138, 5015–5026.
- Masaki, S., 1960. Thermal relations of diapause in the eggs of certain crickets (Orthoptera: Gryllidae). *Bull. Fac. Agric. Hirosaki Univ.* 6, 5–20.
- Mito, T., Kobayashi, C., Sarashina, I., Zhang, H., Shinahara, W., Miyawaki, K., Shinmyo, Y., Ohuchi, H., Noji, S., 2007. *even-skipped* has gap-like, pair-rule-like, and segmental functions in the cricket *Gryllus bimaculatus*, a basal, intermediate germ insect (Orthoptera). *Dev. Biol.* 303, 202–213.
- Mito, T., Noji, S., 2009. *The Two-Spotted Cricket Gryllus bimaculatus: An Emerging Model for Developmental and Regeneration Studies, Emerging Model Organisms: A Laboratory Manual*. Cold Spring Harbor Laboratory Press, Cold Spring Harbor, pp. 331–346.
- Mito, T., Okamoto, H., Shinahara, W., Shinmyo, Y., Miyawaki, K., Ohuchi, H., Noji, S., 2006. *Kruppel* acts as a gap gene regulating expression of *hunchback* and *even-skipped* in the intermediate germ cricket *Gryllus bimaculatus*. *Dev. Biol.* 294, 471–481.
- Mito, T., Ronco, M., Uda, T., Nakamura, T., Ohuchi, H., Noji, S., 2008. Divergent and conserved roles of extradenticle in body segmentation and appendage formation, respectively, in the cricket *Gryllus bimaculatus*. *Dev. Biol.* 313, 67–79.
- Mito, T., Sarashina, I., Zhang, H., Iwahashi, A., Okamoto, H., Miyawaki, K., Shinmyo, Y., Ohuchi, H., Noji, S., 2005. Non-canonical functions of *hunchback* in segment patterning of the intermediate germ cricket *Gryllus bimaculatus*. *Development* 132, 2069–2079.
- Mito, T., Shinmyo, Y., Kurita, K., Nakamura, T., Ohuchi, H., Noji, S., 2011. Ancestral functions of Delta/Notch signaling in the formation of body and leg segments in the cricket *Gryllus bimaculatus*. *Development* 138, 3823–3833.
- Miyawaki, K., Inoue, Y., Mito, T., Fujimoto, T., Matsushima, K., Shinmyo, Y., Ohuchi, H., Noji, S., 2002. Expression patterns of *aristales* in developing appendages of *Gryllus bimaculatus* (cricket). *Mech. Dev.* 113, 181–184.
- Miyawaki, K., Mito, T., Sarashina, I., Zhang, H., Shinmyo, Y., Ohuchi, H., Noji, S., 2004. Involvement of Wingless/Armadillo signaling in the posterior sequential segmentation in the cricket, *Gryllus bimaculatus* (Orthoptera), as revealed by RNAi analysis. *Mech. Dev.* 121, 119–130.
- Nakamura, T., Mito, T., Bando, T., Ohuchi, H., Noji, S., 2008a. Dissecting insect leg regeneration through RNA interference. *Cell. Mol. Life Sci.* 65, 64–72.
- Nakamura, T., Mito, T., Miyawaki, K., Ohuchi, H., Noji, S., 2008b. EGFR signaling is required for re-establishing the proximodistal axis during distal leg regeneration in the cricket *Gryllus bimaculatus* nymph. *Dev. Biol.* 319, 46–55.
- Nakamura, T., Yoshizaki, M., Ogawa, S., Okamoto, H., Shinmyo, Y., Bando, T., Ohuchi, H., Noji, S., Mito, T., 2010. Imaging of transgenic cricket embryos reveals cell movements consistent with a syncytial patterning mechanism. *Curr. Biol.* 20, 1641–1647.
- Niwa, N., Inoue, Y., Nozawa, A., Saito, M., Misumi, Y., Ohuchi, H., Yoshioka, H., Noji, S., 2000. Correlation of diversity of leg morphology in *Gryllus bimaculatus* (cricket) with divergence in *dpp* expression pattern during leg development. *Development* 127, 4373–4381.
- Niwa, N., Saitoh, M., Ohuchi, H., Yoshioka, H., Noji, S., 1997. Correlation between distal-less expression patterns and structures of appendages in development of the two-spotted cricket, *Gryllus bimaculatus*. *Zool. Sci.* 14, 115–125.
- Panfili, K.A., 2008. Extraembryonic development in insects and the acrobatics of blastokinesis. *Dev. Biol.* 313, 471–491.
- Patel, N.H., Kornberg, T., Goodman, C.S., 1989. Expression of *engrailed* during segmentation in grasshopper and crayfish. *Development*, 201–212.
- Rakshpal, R., 1962. Morphogenesis and embryonic membranes of *Gryllus assimilis* (Fabricius) (Orthoptera: Gryllidae). *Proc. R. Entomol. Soc. Lond. Ser. A* 37, 1–12.
- Riegert, P.W., 1961. Embryological development of a nondiapause form of *Melanoplus bilitturatus* Walker (Orthoptera: Acrididae). *Can. J. Zool.* 39, 491–494.
- Ronco, M., Uda, T., Mito, T., Minelli, A., Noji, S., Klingler, M., 2008. Antenna and all gnathal appendages are similarly transformed by homothorax knock-down in the cricket *Gryllus bimaculatus*. *Dev. Biol.* 313, 80–92.
- Roonwal, M.L., 1936. Studies on the embryology of the African Migratory Locust, *Locusta migratoria migratoides* R. and F.I. the early development, with a new theory of multi-phased gastrulation among insects. *Philos. Trans. R. Soc. Lond. B: Biol. Sci.* 226, 391–421.
- Roonwal, M.L., 1937. Studies on the embryology of the African Migratory Locust, *Locusta migratoria migratoides* Reiche and Frm. II. Organogeny. *Philos. Trans. R. Soc. Lond. B: Biol. Sci.* 227, 175–244.
- Salzen, E.A., 1960. The growth of the locust embryo. *J. Embryol. Exp. Morphol.* 8, 139–162.
- Sander, K., 1997. Pattern formation in insect embryogenesis: the evolution of concepts and mechanisms. *Int. J. Insect Morphol. Embryol.* 25, 349–367.
- Sarashina, I., Mito, T., Saito, M., Uneme, H., Miyawaki, K., Shinmyo, Y., Ohuchi, H., Noji, S., 2005. Location of micropyles and early embryonic development of the two-spotted cricket *Gryllus bimaculatus* (Insecta, Orthoptera). *Dev. Growth Differ.* 47, 99–108.
- Sato, M., Tanaka-Sato, H., 2002. Fertilization, syngamy, and early embryonic development in the cricket *Gryllus bimaculatus* (De Geer). *J. Morphol.* 254, 266–271.
- Sauer, G., 1961. Die Regulationsbefähigung des Keimanlagenblastoderms von *Gryllus domesticus* beim Beginn der Wirkung des Differenzierungszentrums. *Zoologische Jahrbucher. Abteilung für Anatomie und Ontogenie der Tiere* 79, 149–222.
- Shinmyo, Y., Mito, T., Matsushima, T., Sarashina, I., Miyawaki, K., Ohuchi, H., Noji, S., 2005. Caudal is required for gnathal and thoracic patterning and for posterior elongation in the intermediate-germ cricket *Gryllus bimaculatus*. *Mech. Dev.* 122, 231–239.
- Slifer, E., King, R., 1934. Insect development VII. Early stages in the development of grasshopper eggs of known age and with a known temperature history. *J. Morphol.* 56, 593–601.
- Slifer, E.H., 1932. Insect development. IV. External morphology of grasshopper embryos of known age and with a known temperature history. *J. Morphol.* 53, 1–21.

- Watanabe, T., Noji, S., Mito, T., 2014. Gene knockout by targeted mutagenesis in a hemimetabolous insect, the two-spotted cricket *Gryllus bimaculatus*, using TALENs. *Methods* 69, 17–21.
- Watanabe, T., Ochiai, H., Sakuma, T., Horch, H.W., Hamaguchi, N., Nakamura, T., Bando, T., Ohuchi, H., Yamamoto, T., Noji, S., Mito, T., 2012. Non-transgenic genome modifications in a hemimetabolous insect using zinc-finger and TAL effector nucleases. *Nat. Commun.* 3, 1017.
- Wheeler, W.M., 1893. A contribution to insect morphology. *J. Morphol.* 8, 1–160.
- Zeng, V., Ewen-Campen, B., Horch, H.W., Roth, S., Mito, T., Extavour, C., 2013. Gene discovery in a hemimetabolous insect: *de novo* annotation and assembly of a transcriptome for the cricket *Gryllus bimaculatus*. *PLoS One* 8, e61479.
- Zhang, H., Shinmyo, Y., Mito, T., Miyawaki, K., Sarashina, I., Ohuchi, H., Noji, S., 2005. Expression patterns of the homeotic genes *Scr*, *Antp*, *Ubx*, and *abd-A* during embryogenesis of the cricket *Gryllus bimaculatus*. *Gene Expr. Patterns* 5, 491–502.